VIROLOGY

Structural basis for recruitment of host CypA and E3 ubiquitin ligase by maedi-visna virus Vif

Yingxia Hu[1], Ragna B. Gudnadóttir[2], Kirsten M. Knecht[1], Fidel Arizaga[1], Stefán R. Jónsson[2], Yong Xiong[1]*

Lentiviral Vif molecules target the host antiviral APOBEC3 proteins for destruction in cellular ubiquitin-proteasome pathways. Different lentiviral Vifs have evolved to use the same canonical E3 ubiquitin ligase complexes, along with distinct noncanonical host cofactors for their activities. Unlike primate lentiviral Vif, which recruits CBFβ as the noncanonical cofactor, nonprimate lentiviral Vif proteins have developed different cofactor recruitment mechanisms. Maedi-visna virus (MVV) sequesters CypA as the noncanonical cofactor for the Vif-mediated ubiquitination of ovine APOBEC3s. Here, we report the cryo–electron microscopy structure of MVV Vif in complex with CypA and E3 ligase components. The structure, along with our biochemical and functional analysis, reveals both conserved and unique structural elements of MVV Vif and its common and distinct interaction modes with various cognate cellular proteins, providing a further understanding of the evolutionary relationship between lentiviral Vifs and the molecular mechanisms by which they capture different host cofactors for immune evasion activities.

INTRODUCTION

To infect and survive in mammalian host cells, lentiviruses have developed multiple mechanisms to overcome host restrictions at various stages of the viral replication cycle (*1*, *2*). Nearly all lentiviruses share a common mechanism, which involves the recruitment of host cellular protein degradation machinery by a conserved viral protein known as virion infectivity factor (Vif) to degrade the host antiviral restriction factors, such as the APOBEC3 (apolipoprotein B mRNA-editing catalytic polypeptide-like 3, A3) family of proteins (*3*–*7*). A3 proteins are deoxycytidine deaminases that potently inhibit lentiviral infections by hypermutating the viral genome and blocking reverse transcription in the absence of Vif (*8*). Different mammals have varying numbers of A3 genes (e.g., seven in human and three in sheep), each with one or two zinc-containing deaminase–like domains that are classified into three distinct phylogenetic groups called Z1, Z2, or Z3 (*9*). The three A3 genes in sheep encode at least four A3 proteins: OaA3Z1, OaA3Z2, OaA3Z3, and the di-domain OaA3Z2Z3 (*10*), with OaA3Z3 corresponding to human A3H and OaA3Z2Z3 functioning as human A3F and A3G (*11*). It has been found that the Vif-A3 interactions are promiscuous; Vif from the sheep-infecting maedi-visna virus (MVV) can degrade not only OaA3Z3 but also other A3Z3-type proteins, such as human A3H, while Vif molecules from human immunodeficiency virus (HIV), bovine immunodeficiency virus (BIV), and feline immunodeficiency virus (FIV) specifically target the Z3-type A3s of their cognate hosts (*12*).

Despite little sequence conservation, lentiviral Vifs recruit highly conserved host Cullin-RING E3 ligase (CRL) complexes (*13*). The multicomponent CRL complexes are composed of the scaffold protein Cullin, the E2-activating RING finger protein Rbx1/2, and adaptor proteins that connect the substrate receptor to Cullin (*4*). While there are a variety of Cullin proteins with different adaptor components, HIV-1 and MVV/caprine arthritis encephalitis virus (CAEV) Vif molecules primarily bind to the Cul5 or Cul2 E3 ligase with adaptor proteins Elongin B (EloB) and Elongin C (EloC) (*13*–*17*). In contrast to the conserved function of recruiting CRL complexes to initiate A3 degradation, different lentiviral Vifs have evolved to recruit divergent cellular partners as noncanonical E3 ligase cofactors. Primate lentiviral Vif proteins recruit CBFβ, which endogenously forms a heterodimer with the transcription factor RUNX1 to control expression of genes implicated in many cellular processes (*18*). However, CBFβ is dispensable for nonprimate Vifs. BIV Vif does not require a cellular cofactor for its activity, while MVV and CAEV Vifs require the noncanonical cofactor cyclophilin A (CypA) to form stable E3 ligase complexes for A3 degradation (*19*, *20*). CypA belongs to the highly conserved cyclophilin family, is a prolyl isomerase that catalyzes the *cis-trans* isomerization of prolyl peptide bonds, and is ubiquitous in both eukaryotic and prokaryotic cells (*21*). It plays critical roles in regulating immune responses in cells and is also a cofactor for HIV-1 infection in multiple aspects of the HIV-1 life cycle (*22*), such as interacting with HIV-1 capsid (*23*). Acetylation of CypA at residue K125 occurs in human cells but not in *Escherichia coli* cells, which has been reported to substantially inhibit CypA catalysis of *cis-trans* isomerization, modulating key functions of CypA in immunity and viral infection (*24*). Both CBFβ and CypA are present and are each highly conserved in mammals; the divergence in cofactor selection by different lentiviral Vifs may therefore point to distinct structural and functional features of Vif proteins and the A3 proteins they target.

To date, crystal structures have been determined for Vif proteins from two primate lentiviruses [HIV-1 and simian immunodeficiency virus isolated from red-capped mangabey (SIVrcm)] in complex with CBFβ and Cul5 E3 ligase components. These structures substantially advance our understanding of how primate lentiviral Vifs recruit CBFβ and Cul5 E3 ligase machinery to degrade A3s (*25*, *26*). However, the molecular mechanisms by which nonprimate lentiviral Vifs have evolved to interact with divergent cellular cofactors and

[1]Department of Molecular Biophysics and Biochemistry, Yale University, New Haven, CT, USA. [2]Institute for Experimental Pathology, University of Iceland, Keldur, Reykjavik 112, Iceland.
*Corresponding author. Email: yong.xiong@yale.edu

cognate E3 ligases are largely unknown. In this study, we report a high-resolution cryo–electron microscopy (cryo-EM) structure of MVV Vif in complex with CypA and the EloB/C components of the Cul5 E3 ligase complex. In combination with biochemical and cellular functional studies, our structure reveals both conserved and previously unknown features of MVV Vif, and the molecular mechanism of how it interacts with the E3 ligase components and the noncanonical cofactor CypA. The results highlight the important similarities and differences between MVV Vif and primate lentiviral Vif proteins, providing substantial insight into the molecular determinants that have driven the divergent strategies of different lentiviruses evolved in adaption to the A3 suppressions.

RESULTS

To obtain the structure of MVV Vif in complex with its host cofactor and E3 ligase, we first assembled the complex of $Vif_{18\text{-}230}$/CypA/EloB/EloC (VCBC), which was purified as a monodispersed complex (*27*) but did not give a high-resolution cryo-EM structure, partly because of its small size (~70 kDa total) and instability. We then assembled a VCBC fusion complex by linking CypA to $Vif_{18\text{-}230}$ with a 30–amino acid linker to stabilize their interaction, which unexpectedly resulted in the dimerization of the VCBC complex (fig. S1A). By further stabilizing the dimerization under cryo condition through chemical cross-linking with the BS3 cross-linker (fig. S1B), we obtained a cryo-EM reconstruction of the VCBC dimer in C2 symmetry at a resolution of 3.5 Å (Fig. 1A, left). The high-quality cryo-EM map allowed for the modeling of the entire MVV Vif construct (residues 18 to 230), residues 2 to 164 of CypA (of 165 amino acids total), and most of EloB and EloC (except for two disordered loops).

Lentiviral Vif molecules define distinct structures with cellular cofactors

The overall VCBC structure has a butterfly-shaped architecture, with the dimerized Vif forming the central body and CypA and EloB/C forming the lower and upper wings, respectively (Fig. 1A, right). EloB/C is recruited to MVV Vif at the conserved BC-box interface in the same way as that to HIV-1 Vif. By contrast, the noncanonical cofactor CypA contacts MVV Vif at an opposite side from which CBFβ interacts with HIV-1 Vif (Fig. 1B). A comparison of the quaternary MVV and HIV-1 VCBC structures suggests that lentiviral Vif plays a central role in defining the complex architecture (Fig. 1B). A linear alignment of the secondary structure elements indicates that HIV-1 and MVV Vif have evolved to form more divergent N-terminal and C-terminal sequences while retaining relatively conserved core regions (fig. S2). This is also consistent with what we observed structurally. The core of MVV Vif without its N and C termini adopts a domain architecture similar to that of primate lentiviral Vifs (*25*, *26*), which can be divided into an α domain and an α/β domain, but with a different relative orientation between the two domains (Fig. 2, A and B). When the α domains of MVV Vif and HIV-1 Vif are overlaid, the five-stranded antiparallel β sheet in the α/β domain of MVV Vif has a nearly 90° twist away from that of HIV-1 Vif. Despite the large orientation difference, a conserved zinc-binding site coordinated by a zinc finger motif (CCCC for MVV Vif and HCCH for HIV-1 Vif) (*14*, *27*–*29*) stabilizes the interdomain loops between the two domains in a similar fashion in the two Vif structures (Fig. 2A).

Different from the relatively conserved core structure, the N and C termini of MVV Vif are evolutionarily divergent from those of HIV-1 Vif. The N- and C-terminal α helices (α1 and α6) of HIV-1 Vif tightly pack against the Vif core β sheet to form part of the α/β domain, while the N-terminal β strand protrudes and cofolds into the β sheet in the core of CBFβ (Fig. 2A, left) (*25*). By contrast, the N-terminal α helix (α1) and loop region of MVV Vif swings out from the α/β domain for CypA binding (Fig. 2A, right), while a long C-terminal loop region of MVV Vif, which is absent in the previously determined primate lentiviral Vif structures (*25*, *26*), packs onto the α/β domain to form part of the core domain (Fig. 2A, right). In addition, the C-terminal α helix (α8) of MVV Vif is sandwiched between the α and α/β domains to stabilize the overall structure of the molecule (Fig. 2A, right).

MVV Vif recruits the Cul5 E3 ligase through a conserved interface

In addition to the two loosely packed α helices conserved in primate lentiviral Vifs (*25*, *26*), the α domain of MVV Vif has another α helix (α5) that directly contacts the α/β domain (Fig. 2, A, right, and B). This α helix, which is longer than that (α4) of primate lentiviral Vifs and packs more tightly with the other two α helices (Fig. 2B), would clash with the C-terminal tail of CBFβ when overlaid onto the HIV-1 VCBC structure (Fig. 2C). This may partially explain why MVV Vif does not use CBFβ as a cofactor. The positioning of the three α helices is further stabilized by a zinc finger motif connecting the interdomain loops (Fig. 2A, right). Similar to other lentiviral Vifs, MVV Vif contains a conserved BC-box motif (SLQ) in its α domain responsible for recruiting the EloB/C components of the E3 ligase (Fig. 3). Superposition of EloB/C subunits of MVV VCBC and the HIV-1 VCBC/Cul5 complex structures indicates that MVV Vif also interacts with the Cul5 scaffold through a conserved IR motif in the α domain (Fig. 3), consistent with the previous mutagenesis results on the role of this motif in Cul5 interaction (*17*, *27*).

MVV Vif recruits the noncanonical CypA through a unique hook-like interface

Although MVV Vif shares a binding interface common to that of HIV-1 Vif for interaction with the Cul5 E3 ligase, it recruits the noncanonical host cofactor CypA in a distinct manner. Unlike primate lentiviral Vifs that bind CBFβ via a hydrophobic surface in its α/β domain (*25*, *26*), MVV Vif interacts with CypA through a surface located on the opposite side of the viral molecule, stabilized by both electrostatic and hydrophobic interactions (Fig. 4A). A hook-like structure formed by the extended N-terminal region and the α domain of MVV Vif core engages CypA tightly (Fig. 4B), burying a total surface area of 2752 $Å^2$. Despite the completely different spatial and structural configurations, both HIV-1 and MVV Vifs have their N termini extend into the cognate host cofactors. The bound CypA cofactor adopts the same structure as that of the apo molecule (root mean square deviation of ~0.9 Å).

The N-terminal region of MVV Vif forms the "head" of the CypA hook, clasping CypA and reaching into its catalytic site. It is composed of a long U-turn loop connecting to a long α helix (Fig. 4B). The CypA substrate motif (^{21}PxxP^{24}) at the tip of the Vif loop interacts with the catalytic site of CypA in a canonical manner and, together with the α helix, tightly cradles CypA

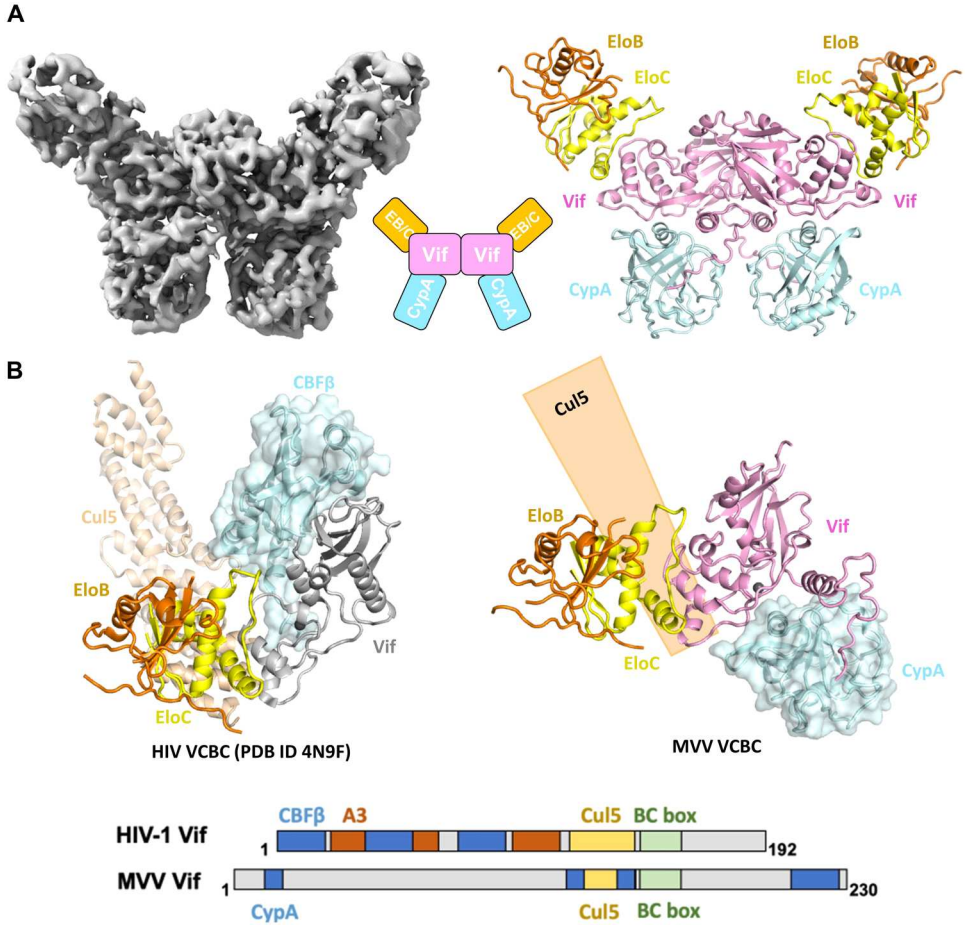

Fig. 1. Overall structure of MVV Vif in complex with CypA and EloB/C (VCBC). (**A**) Cryo-EM map (left) and the atomic model (right, ribbon representation) of the butterfly-shaped dimerized MVV VCBC complex. The middle inset shows a cartoon illustration of the complex. (**B**) Top: Structural comparison of HIV-1 VCBC with Cul5 N-terminal domain (left) and MVV VCBC (right). Bottom: Domain/motif comparison of HIV-1 and MVV Vif proteins for regions interacting with different host proteins.

(Fig. 4C, bottom middle and left). The interaction between CypA and the ^{21}PxxP^{24} motif of MVV Vif is similar to those with cellular substrates and viral partners, such as the HIV-1 capsid protein (CA) (*23*, *24*). P21 of MVV Vif stacks onto CypA F113, P24 forms a modest packing interaction with CypA F60, and the peptide carbonyls of G20 and L23 point toward a positively charged patch on CypA consisting of K125 and H126 (Fig. 4C, bottom left). These interactions substantiate the previous findings from biochemical and nuclear magnetic resonance experiments that the MVV Vif ^{21}PxxP^{24} motif directly binds to the active site of CypA (*19*). Both proline residues were detected in the *trans* isoform. The direct engagement of the CypA catalytic site in MVV Vif binding supports the prior report that the *cis-trans* prolyl isomerase activity of CypA may be important for MVV Vif function (*19*), although the exact role of the catalytic activity of CypA in OaA3Z2Z3 degradation remains elusive. The interaction mode of MVV Vif ^{21}PxxP^{24} motif with CypA is in between those observed for HIV-1 CA interactions with unacetylated (*23*) and acetylated (*24*) CypA, although in this study the protein was produced in *E. coli* and there was no acetylation detected.

Furthermore, W121 of CypA interacts with the "bend" of the hook via hydrophobic contacts with Vif P24/L25 of the PxxP motif and L47/L50 situated at the center of the long α helix (Fig. 4C, bottom left and middle). We carried out mutagenesis study in vitro and in cells to further verify the new interactions observed from the MVV VCBC structure. Mutating either Vif L47/L50 or CypA W121 did not affect the protein solubility and Vif interaction with EloB/C (Fig. 5A), indicating that the mutations did not impair proper protein folding. However, they readily disrupted the binding between Vif and CypA in vitro (Fig. 5A), and the Vif L47D/L50D double mutation rendered OaA3Z2Z3 resistant to Vif-mediated degradation in cells (Fig. 5B), supporting the biological importance of these residues in Vif-CypA interaction.

The interdomain loop region and the α domain of MVV Vif form the "shank" of the hook to provide another important binding surface for CypA. The MVV Vif interdomain loop region and the CCCC zinc finger motif form the upper half of the hook shank, which interacts with the α helix adjacent to the C terminus of CypA through both hydrophobic and electrostatic interactions (Fig. 4C, top left and bottom right). This explains why the zinc finger motif was found to be important for CpyA binding and OaA3Z2Z3 degradation (*27*). Mutating either Vif R55 or CypA E140/E143, which neutralizes with each other at this interface (Fig. 4C, bottom right), also abolished the Vif-CypA binding in

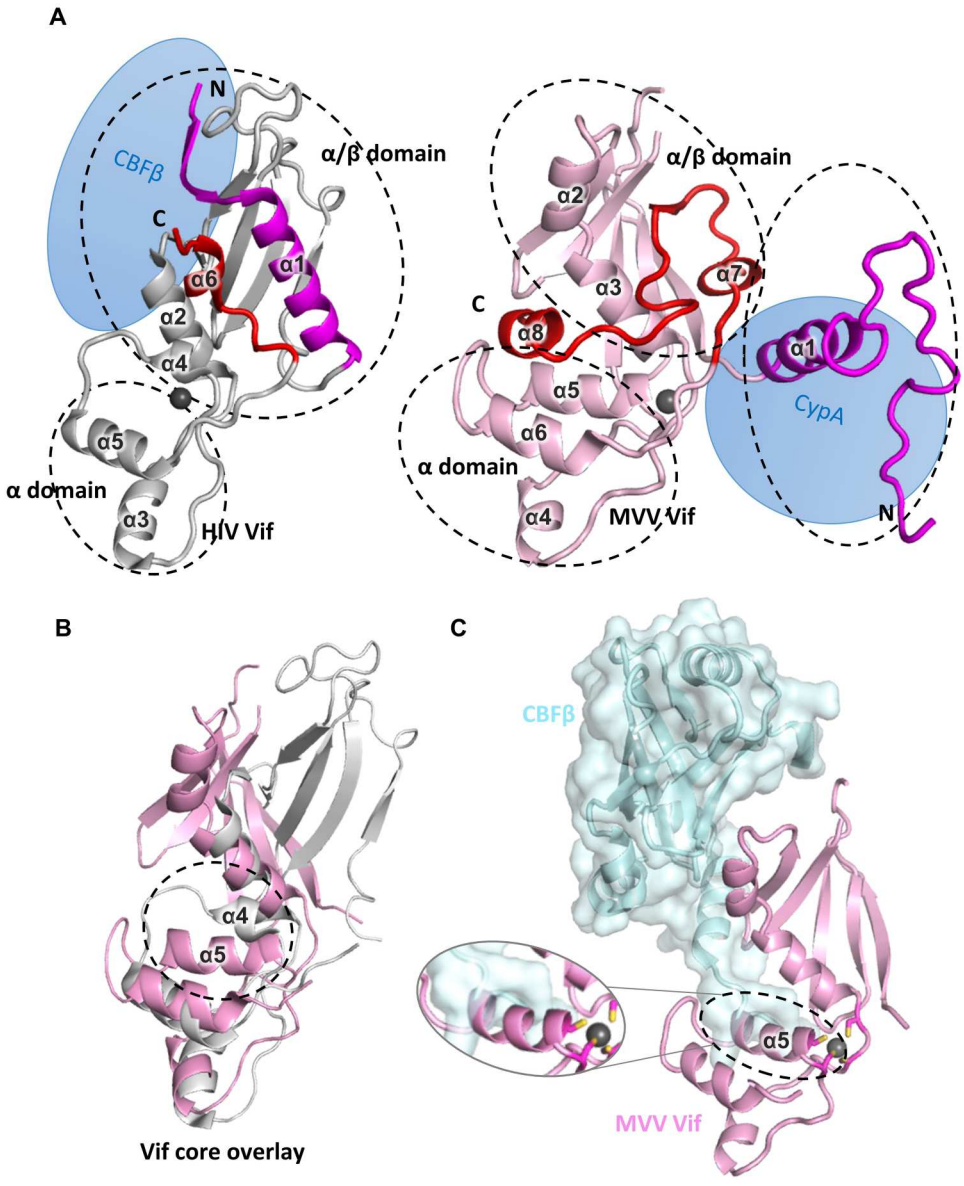

Fig. 2. Domain structure of MVV Vif and its comparison with HIV-1 Vif. (**A**) Side-by-side comparison of HIV-1 and MVV Vif structures and their respective interactions with noncanonical host cofactors (blue ovals). Both Vif molecules have conserved domain architectures, with the more variable N- and C-terminal regions highlighted in magenta and red. The zinc atoms are shown as gray spheres. (**B**) Superposition of HIV-1 (gray) and MVV (magenta) Vif core structures. Deviation of the α helix at the domain interface is marked by an oval. (**C**) Superposition of MVV Vif onto HIV-1 Vif/CBFβ reveals spatial clashes between CBFβ C-terminal tail and an α helix (marked by an oval, inset) from the α domain of MVV Vif.

vitro and substantially inhibited the Vif-mediated OaA3Z2Z3 degradation in cells (Fig. 5, A and B). At the lower half of the hook shank, W154 from the Vif α domain packs against a CypA hydrophobic patch containing V12/L17/F145 next to the C-terminal α helix (Fig. 4C, top left). Mutation of either Vif W154A or the CypA hydrophobic patch (V12A/L17A/F145A) significantly reduced the Vif-CypA interaction in vitro (Fig. 5A). The Vif W154A mutant also led to severe deficiency in OaA3Z2Z3 degradation in cells (Fig. 5B). At the end of the hook shank, there is also a positively charged surface constituted by Vif K151 and surrounding backbone amino groups that complement a negatively charged convex surface formed by CypA E15 and adjacent backbone carbonyl groups (Fig. 4C, top middle).

Besides residues directly involved in CypA interactions, the C-terminal α helix of Vif plays an important role shaping the interaction interface. It was found to be essential for CpyA binding and OaA3Z2Z3 neutralization (*27*). As shown from the structure, it is not located at the CpyA-binding interface but indirectly affects the CypA binding through a long interdomain loop (Fig. 4C, top right). Mutating one residue of the interdomain loop, P192, which is sandwiched by the Vif N-terminal helix and C-terminal loop, has been reported to completely abrogate the Vif-CypA interaction (*19*). Moreover, the strong negatively charged C-terminal α

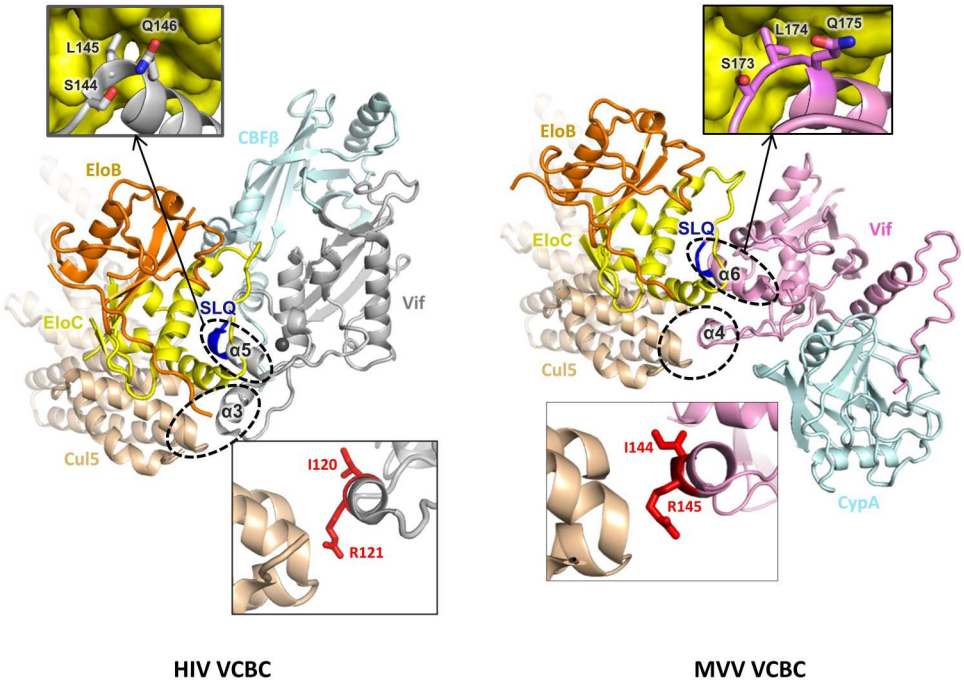

Fig. 3. The conserved binding interface of Vif with the Cul5 E3 ligase. Overlaying the Cul5/EloB/C components of the HIV-1 complex structure onto the EloB/C components of the MVV complex shows that HIV-1 and MVV Vifs share a conserved BC-box interface (top, zoomed-in insets) for interaction with the EloB/C components of E3 ligase, and both Vif molecules have a similar interface containing an IR motif (bottom, zoomed-in insets) for Cul5 interaction.

helix bridges the two domains of the Vif core through electrostatic interactions (Fig. 4C, top middle), thus stabilizing the overall architecture of MVV Vif. Truncation of the C-terminal region would affect the overall protein folding, which in turn would disrupt the Vif-CypA interaction.

DISCUSSION

Lentiviruses infect a variety of mammalian hosts and have evolved lineage-specific mechanisms to overcome their cognate host challenges. In lentiviral Vif–mediated degradation of host A3 proteins, the recruited host CRL complexes are highly conserved among different species, leading to an evolutionarily conserved mechanism by which Vif proteins interact with the CRL complexes. This has been supported by comparing our nonprimate MVV VCBC structure with the available primate HIV-1 and SIVrcm VCBC structures (*25*, *26*). The Vif α domains in these structures, which are responsible for recruiting the host CRL complex, have highly similar binding interfaces for EloC/Cul5 with modest local variations. The HIV-1 and MVV Vifs may also share analogous binding surfaces, with some variations, for recruiting cognate Z3-type A3s (fig. S3A). HIV-1 Vif has been predicted to bind human A3H through the concave surface of its β sheet [reviewed in (*30*)]. MVV Vif is promiscuous and degrades not only sheep A3Z3 but also the A3Z3-type proteins of other species, including human (*12*). Previous study has observed that mutation of W98 from the similar β sheet concave surface of MVV Vif impaired its ability to antagonize OaA3Z2Z3 (*31*). W98 is located near a positively charged surface (fig. S3B, left) that is complementary to the predicted negatively charged Vif-binding surface of human A3H (fig. S3B, right). We carried out in vitro binding assay using human A3H to investigate the potential MVV Vif–binding interface for Z3-type A3s. We also compared the unfused monomeric MVV VCBC complex and the fused dimeric VCBC complex in their abilities to bind human A3H. The results showed that the fusion dimer did not substantially affect A3H binding (fig. S3C, left). The OaA3Z2Z3 degradation–deficient MVV Vif W98R mutation did not have apparent effects on human A3H recruitment to the VCBC complex (fig. S3C, right), indicating that MVV Vif may have somewhat different binding interfaces for human A3H and sheep OaA3Z2Z3.

We determined cryo-EM structure of the VCBC complex in a dimeric form. Although we could not rule out the biological relevance of the dimeric complex, several lines of evidence suggest that dimerization is not likely needed functionally. First, the observed VCBC dimer was mediated by positively charged surfaces on both MVV Vif protomers (fig. S3B, left) and needed to be stabilized by BS3 chemical cross-linking. It is possible that BS3 cross-linked the protomers to mitigate charge repulsion, or charge neutralization by the reacted BS3 molecules stabilized the dimer without cross-linking. Second, dimerization only occurred when the MVV Vif–CypA fusion construct was used, but not with the unfused proteins. The fusion linker introduced between CypA and Vif was not visible in the cryo-EM map; therefore, we could not rule out a domain-swapped dimer (fig. S4). The distance between the fusion points in one monomeric VCBC complex structure is ~36 Å (fig. S4, right), which would need a linker length of more than 50 Å to bridge as they are on the opposite side of CypA. On the other hand, a domain-swapped configuration requires a linker distance of more than 35 Å (fig. S4, left). The 30–amino acid linker in the fusion construct can span more than 100 Å in the most extended conformation (i.e., β-strand geometry), which can permit either scenario. Third, regardless of the dimerization mode, the observed MVV Vif–CypA

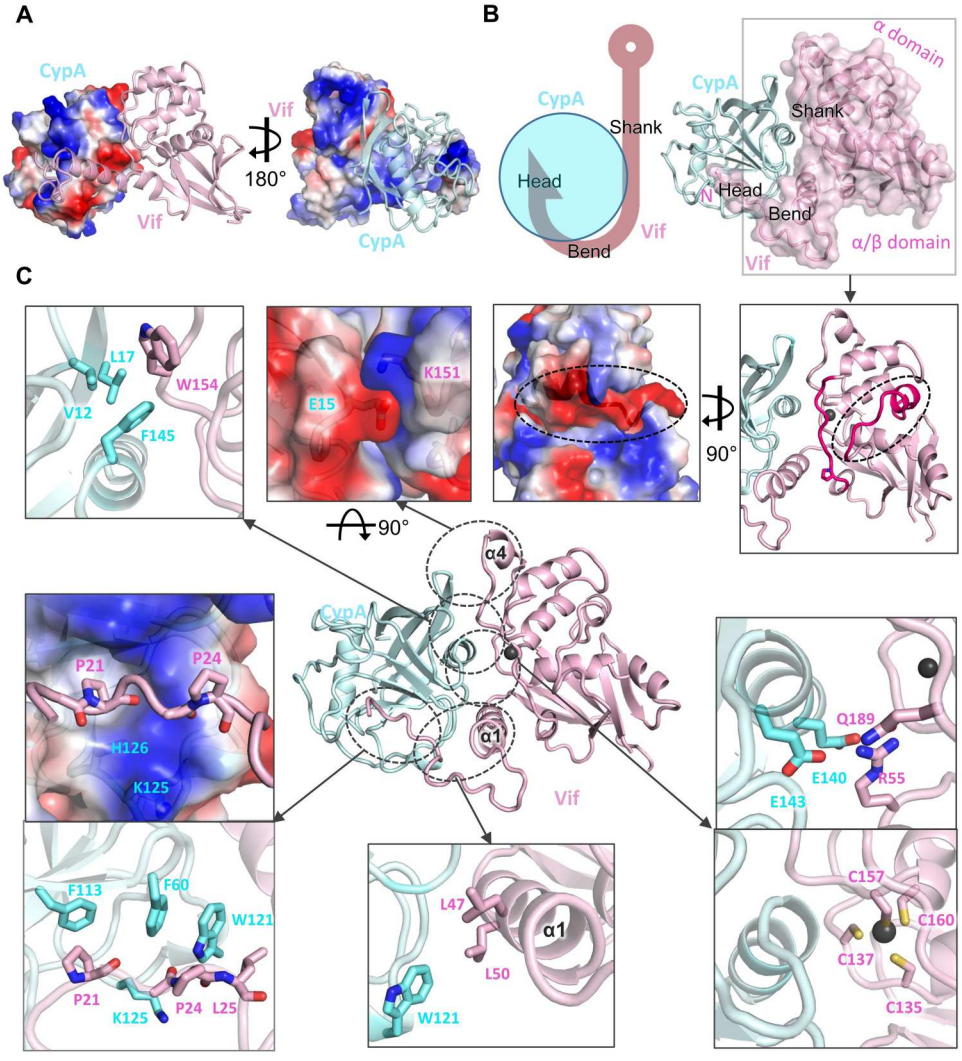

Fig. 4. The unique binding interface for MVV Vif interaction with CypA. (**A**) Overall surface electrostatic potential of the Vif-CypA interface. Blue, positively charged; red, negatively charged. (**B**) Overview and cartoon representation of the hook-like Vif-CypA interface, which can be divided into the head, bend, and the shank of the hook. (**C**) Detailed illustrations for important MVV Vif–CpyA interactions observed in the MVV VCBC complex structure. In addition to direct interactions, the C-terminal tail of MVV Vif (top right), which is marked by an oval and colored in pink, indirectly interferes with the CypA interaction through a long interdomain loop, which is also colored in pink.

interface explained extensive previous biochemical and functional data and was further validated in this study with unfused construct that does not dimerize. These observations suggest that the observed interface faithfully captured the physiological interaction when dimer formation may not occur.

In contrast to the largely conserved modes of interactions with CRL and A3 substrates, Vif proteins of different viral lineages have exhibited diversity in recruiting noncanonical host cofactors to exert their functions. Human and sheep both possess CBFβ and CypA, which have no structural or functional resemblance to each other, but each is strictly conserved between the two hosts (>99% identity in amino acid sequences). However, evolutionally, HIV-1 and MVV/CAEV have selected only one of the two unrelated host cofactors for stabilizing Vif and preserving their cellular activities. The variations in Vif proteins themselves could be one determinant leading to this divergent adaption. Structurally, despite maintaining a conserved overall Vif core structure as that of HIV-1 Vif, the different relative orientation between the α/β and α domains of MVV Vif results in a more compact interface for host cellular proteins and may cause spatial clashes for EloC/Cul5 and CBFβ to bind. Besides, the more variable N- and C-terminal regions of Vif proteins generate distinct protein-interacting surfaces, which may allow for selection of different host cofactors during evolution. CBFβ and CypA bind to opposite sides of the cognate Vif molecule with different surface compositions and charge properties —CBFβ primarily interacts with the α/β domain of HIV-1 Vif, while CypA mainly interacts with the α domain and the extended N-terminal regions of MVV Vif. An interesting commonality is that the N-terminal regions of both Vif proteins are evolved to interact with the noncanonical host factors.

Host factor engagement by multiple viral proteins in the same virus may be an evolutionary driving force in Vif's selection of

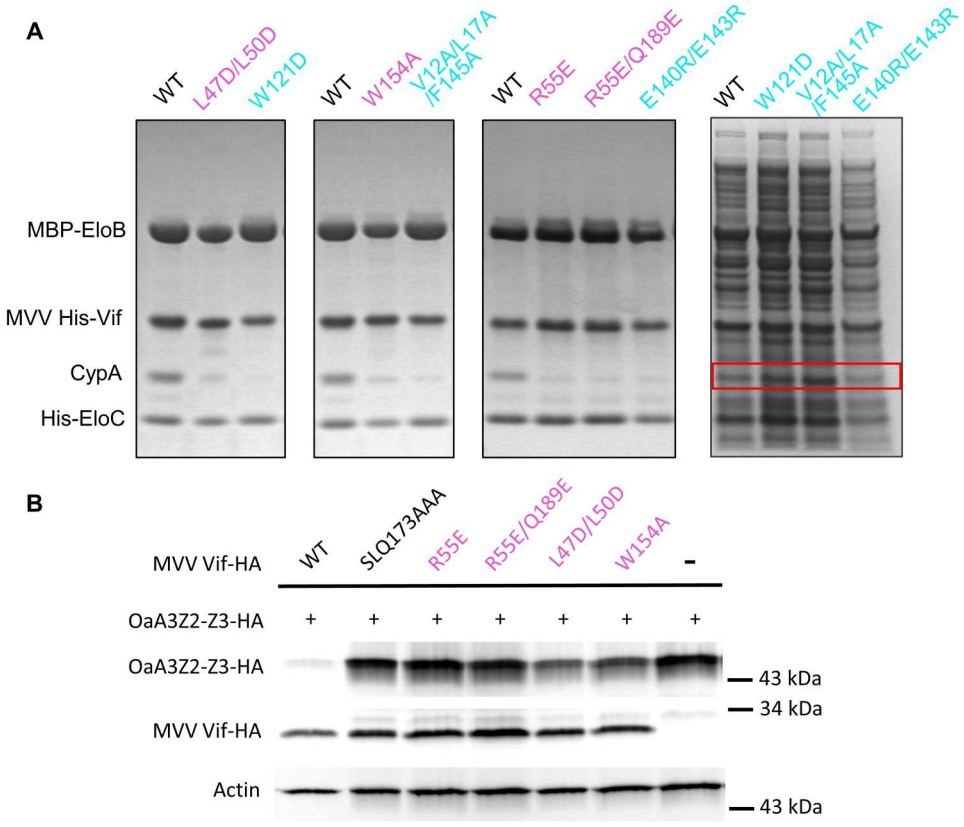

Fig. 5. Mutagenesis validation of the observed MVV Vif-CypA binding interface. (A) In vitro binding analysis of MVV Vif and CypA variants. The mutated residues correspond to the important Vif-CypA interacting residues observed and highlighted in Fig. 4C. Vif variants are labeled in magenta, and those in cyan are CypA variants. All eluates (left, three panels) and the loading controls for CypA mutants (right, with the CypA band marked by a red box) shown in (A) indicate that all Vif and CypA mutants are as soluble as the wild type (WT) proteins. **(B)** Mutational analysis of the critical MVV Vif residues interacting with CypA by Vif-mediated OaA3Z2Z3 degradation assay in cells.

different cofactors. The abundance of a host protein is often a key property that contributes to its recruitment by viruses during viral infection. CypA is highly abundant in virtually all cell types and have been found to be involved in the infections of multiple viruses [reviewed in (*22*)]. In human cells, CypA plays a key role in enhancing HIV-1 infectivity by interacting with the virus capsid protein (CA) (*32*–*34*), which may modulate the stability of the capsid and its access by various other host proteins. The major CypA interaction site of HIV-1 CA constitutes a long flexible loop containing Gly89/Pro90 protruded into the CypA active site. CypA further interacts with multiple CA subunits through other interfaces to enhance binding to the assembled capsid (*34*). It is conceivable that the important CypA-capsid interplays take evolutionary precedence, and HIV-1 Vif has evolved to select another abundant host factor, CBFβ. Theoretically, the cellular abundance of CypA can supply enough cofactors for both CA and Vif to bind, although the requirement of the same host protein by multiple viral proteins would put the virus under a stricter constraint and therefore disadvantageous to viral fitness and adaptation. In addition, the recruitment of CBFβ by HIV-1 Vif interferes with its endogenous association with the transcription factor RUNX1, which controls the expression of immune-related genes, including A3 proteins (*18*), potentially offering another evolutionary advantage for the virus.

By contrast, MVV capsid has been found to have no interaction with CypA (*19*), which may free up the host protein as a cofactor for MVV Vif. A common strategy for viral proteins to recruit host factors is to mimic the endogenous interaction partners, in this case the CypA substrate motif PxxP, which is present in both HIV-1 CA and MVV Vif but absent in HIV-1 Vif. The peptidyl-prolyl isomerase activity of CypA has been found to be critical for MVV Vif–mediated OaA3Z2Z3 degradation without affecting Vif-CypA interaction (*19*). This indicates that there may be a yet unknown effect for the *cis-trans* isomerization of the MVV Vif PxxP motif that is important for viral infectivity. It has been shown that the CypA-mediated *cis-trans* isomerization of HIV-1 CA triggers conformational changes in CA distal to the CypA-interacting loop (*35*), although its role for HIV-1 infectivity is not clear. In addition, our structure reveals that a large additional CypA-binding surface is evolved in MVV Vif, which is consistent with the observation that a much higher concentration of the CypA active-site inhibitor cyclosporine A was required to disrupt the CypA interaction with MVV Vif than that needed to disrupt the interaction between CypA and HIV-1 capsid (*19*).

Overall, our structure allows the visualization of detailed MVV Vif interfaces with CypA and critical E3 ligase components, which, together with the available structures of other Cul5 E3 components (*25*, *36*), offers a complete molecular model for MVV Vif–mediated

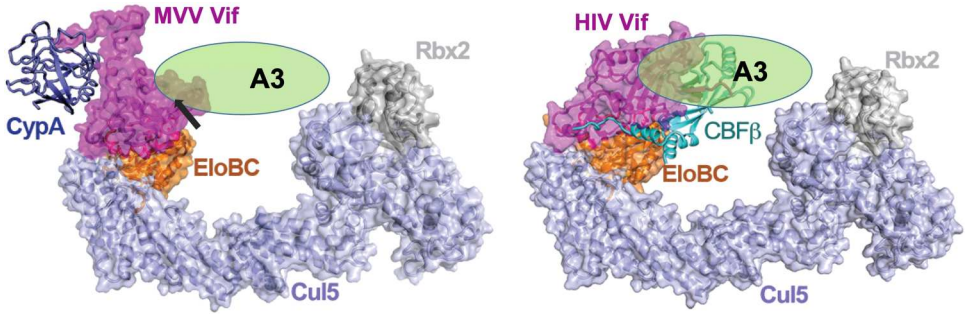

Fig. 6. The comparison of the overall models for Vif-mediated recruitment of A3s to Cul5 E3 ligase by MVV and HIV-1. The complete HIV-1 Vif–CBFβ–Cul5 E3 complex model is constructed by overlaying the Vif-CBFβ-EloB/C-Cul5$_{NTD}$ complex structure (PDB 4N9F) with the separately determined Cul5$_{CTD}$-Rbx2 (PDB 3DPL) structure. The complete MVV Vif–CypA–Cul5 E3 complex model is constructed by overlaying the EloB/C components of the MVV VCBC complex structure onto that of the modeled HIV Vif–CBFβ–Cul5 E3 complex structure. The arrow marks the location of MVV Vif W98 implicated in OaA3Z2Z3 degradation.

recruitment of host ubiquitin E3 ligase (Fig. 6). The model with the complete Cul5 E3 ligase reveals that, unlike CBFβ, which binds HIV-1 Vif at the interface facing Rbx2 and the ubiquitin-carrying E2, CypA binds MVV Vif at the opposite side away from the substrate ubiquitination site, indicating that it is unlikely to participate in direct A3 recruitment. By contrast, the previously reported MVV Vif site containing W98, which is critical for OaA3Z2Z3 degradation, is facing Rbx2 to allow ubiquitination. In summary, our results provide notable insight into the elements that help drive the evolution of lentiviral Vifs to capture their host cofactors, facilitating future studies for a more comprehensive understanding of these complex host-virus interplays.

MATERIALS AND METHODS

Plasmid construction

The 6×His-tagged MVV Vif residues 1 to 230 and human CypA residues 1 to 165 were cloned into the pETDuet vector. Maltose binding protein (MBP)-tagged EloB residues 1 to 118 and 6×His-tagged EloC residues 17 to 112 were cloned into the pACYCDuet vector. The 6×His-tagged or 6×His-Bril–tagged CypA residues 1 to 165 were fused to MVV Vif residues 18 to 230 through a 30–amino acid linker (GSDEASEASELACPTPKEDGLAQQRGSGSG) (CypA-30-Vif18) to stabilize the Vif-CypA binding. EloB residues 1 to 102 and EloC residues 17 to 112 were cloned into the pACYCDuet vector. The 6×His-mCherry–tagged human A3H was cloned into the pETDuet vector. All Duet vectors were from Novagen Inc. All Vif and CypA mutants were constructed following the protocol of the QuikChange II Site-Directed Mutagenesis Kit (Agilent Technologies).

Protein expression and purification

The *E. coli* BL21 (DE3) cells (New England BioLabs) were used for protein expressions. The 6×His-tagged CypA-30-Vif18 and EloB 1–102/EloC 17–112 constructs were coexpressed to obtain the fused MVV VCBC complex for structural study [with MBP-tagged EloB 1–118 and 6×His-tagged EloC 17–112 used for initial complex characterizations (fig. S1A)]. The 6×His-Bril–tagged CypA-30-Vif18 and MBP-tagged EloB 1–118/6×His-tagged EloC 17–112 constructs were coexpressed to obtain the fused Bril-tagged MVV VCBC complex for in vitro binding assay. The 6×His-tagged MVV Vif 1–230/CypA 1–165 and MBP-tagged EloB 1–118/6×His-tagged EloC 17–112 constructs were coexpressed to obtain the unfused MVV VCBC complex for in vitro binding assay. In addition, the 6×His-Bril–tagged human A3H was separately expressed for in vitro binding assay. The protein expressions were induced by 0.3 mM isopropyl-β-D-thiogalactopyranoside (IPTG) at 16°C for 16 hours in Terrific Broth.

Cells were harvested and lysed by a microfluidizer. The lysate was clarified by centrifugation and then applied to a Ni–nitrilotriacetic acid (NTA) (Qiagen) gravity column. The unfused and fused MVV VCBC complexes were then purified by anion exchange (HiTrap Q HP, GE Healthcare) chromatography in a buffer of 30 mM tris and 0.2 mM Tris (2-carboxyethyl) phosphine (TCEP) (pH 8.0) with a gradient NaCl concentration from 20 mM to 1 M and, subsequently, size exclusion chromatography (SEC; HiLoad Superdex 200, GE Healthcare) in a buffer of 30 mM tris, 150 mM NaCl, and 0.2 mM TCEP (pH 8.0). mCherry-A3H was purified in a similar strategy with 0.5 mM deoxyribonuclease/ribonuclease in buffers throughout the procedure and 1 M NaCl in the SEC buffer. Purity of the proteins was analyzed by SDS–polyacrylamide gel electrophoresis (SDS-PAGE) after each step, and the purified proteins were concentrated and stored at −80°C.

Cross-linking of fused MVV VCBC complex

Fused MVV VCBC complex (34 μM) was incubated on ice for 2 hours with 4 mM bissulfosuccinimidyl suberate (BS3, Thermo Fisher Scientific) in buffer of 30 mM NaPi (pH 7.2), 100 mM NaCl, and 0.2 mM TCEP and then quenched by 100 mM tris (pH 7.4). The cross-linked sample was further loaded onto Yarra SEC-3000 (Phenomenex) for separation of the monodispersed MVV VCBC peak. The sample from the peak fraction was used for cryo-EM grid preparation.

Binding assays in vitro

Small-scale expressions of unfused MBP-tagged MVV VCBC wild type (WT) and variants were induced in 50 ml of Terrific Broth by 0.3 mM IPTG at 16°C for 16 hours. Cells were harvested and lysed by sonication. The lysate was clarified by centrifugation and then purified by 50 μl of Ni-NTA (Qiagen) beads in a 1.5-ml Eppendorf tube. The Ni-NTA eluate was further mixed with 50 μl of amylose resin (New England BioLabs) and incubated for 1 hour. After removing the supernatant by centrifugation, the resin was washed with 300 μl of binding buffer [30 mM tris, 100 mM NaCl, and 0.2

Table 1. Cryo-EM data collection, refinement, and validation statistics.

	MVV VCBC
Data collection and processing	
Magnification	81,000
Voltage (kV)	300
Electron exposure (e^{-}/Å^2)	62
Defocus range (μm)	−0.9 to −2
Pixel size (Å)	1.1
Stage tilting (°)	0
Symmetry imposed	C2
Initial particle images (no.)	4,857,569
Final particle images (no.)	74,320
Map resolution (Å)	3.5
FSC threshold	0.143
Map resolution range (Å)	–
Refinement	
Initial model used (PDB code)	3K0N, 3DCG
Model resolution (Å)	3.8
FSC threshold	0.5
Model resolution range (Å)	3.8
Map sharpening *B* factor (Å^2)	0
Model composition	
Nonhydrogen atoms	8854
Protein residues	1100
Ligands	Zn, 2
B factors (Å^2)	
Protein	143
Ligand	128
Root mean square deviations	
Bond lengths (Å)	0.02
Bond angles (°)	0.5
Validation	
MolProbity score	1.83
Clashscore	6.6
Poor rotamers (%)	0
Ramachandran plot	
Favored (%)	92.4
Allowed (%)	7.2
Disallowed (%)	0.4

mM TCEP (pH 8.0)] for three times. Eighty microliters of the elution buffer (binding buffer plus 0.2 mM maltose) was then added to the resin and incubated at 4°C for 10 min before centrifugation. The loading and elution fractions were analyzed by SDS-PAGE.

A total of 0.15 mg of MBP-tagged unfused MVV VCBC or fused Bril-tagged VCBC complexes (0.15 mg) was first incubated with human mCherry-A3H at 1:2 molar ratio in 100 μl of binding buffer containing 30 mM tris, 100 mM NaCl, and 0.2 mM TCEP (pH 8.0) at 4°C for 2 hours, subsequently mixed with 50 μl of amylose resin (New England BioLabs) in 1.5-ml EP tubes, and incubated for one additional hour. The subsequent steps for A3H/VCBC complex purification were the same as above. The loading and elution fractions were analyzed by SDS-PAGE.

A3 degradation assays

Twenty-four–well plates were seeded with 250,000 human embryonic kidney (HEK) 293T cells and transfected the next day using TurboFect (Thermo Fisher Scientific), as specified by the manufacturer. To assay for degradation of ovine A3Z2Z3 by WT MVV Vif and the various mutant Vif proteins, 0.5 μg of pcDNA3.1-OaA3Z2-Z3-HA and 0.5 μg of pVR1012–MVV Vif–HA were used for cotransfection. To maintain equivalent DNA amounts, empty pVR1012 vector DNA was used when needed. After 48 hours, the cells were lysed in 100 μl of lysis buffer [50 mM tris-HCl, 150 mM NaCl, 1 mM EDTA, and 1% Triton X-100 (pH 7.4)] for 20 min followed by 10 min of centrifugation at 10,000 relative centrifugal force and 4°C to clarify lysate. Supernatants were boiled in 6× sample buffer, and a fraction of the samples were run on a 12% SDS-PAGE gel. Proteins were then transferred to a polyvinylidene difluoride membrane (Millipore). Immunoblotting was performed with primary antibodies against the hemagglutinin-tag (ab9110, Abcam) and secondary anti-rabbit or anti-mouse antibodies, which were horseradish peroxidase–conjugated (Cell Signaling Technology), and detection was carried out using with a chemiluminescent horseradish peroxidase antibody detection reagent (Western Blotting Luminol Reagent, Santa Cruz Biotechnology). β-Actin (MAB1501, Millipore) was used as a loading control.

Cryo-EM sample preparation, data collection, and processing

The cross-linked VCBC complex (3 μl) was applied to a homemade graphene-coated C flat 2/1-3C copper grid (Electron Microscopy Sciences) pretreated by ultraviolet ozone for 30 min. The grid was blotted at 4°C with 100% humidity and plunge-frozen in liquid ethane using FEI Vitrobot Mark IV (Thermo Fisher Scientific). The grids were stored in liquid nitrogen before data collection.

Images were acquired on an FEI Titan Krios electron microscope (Thermo Fisher Scientific) equipped with Gatan K3 Summit direct detector in super-resolution mode, at a calibrated magnification of ×81,000 with the physical pixel size corresponding to 1.1 Å. Detailed data collection statistics for the MVV VCBC complex has been indicated in Table 1. Automated data collection was performed using SerialEM (*37*), and a total of 5304 movie series were collected.

Motion correction of each micrograph, contrast transfer function (CTF) estimation, particle picking, two-dimensional (2D) classification, ab initio 3D reconstruction, and nonuniform refinement were carried out by standard pipeline in cryoSPARC (*38*). The dataset consisted of 4,857,569 initial particles, leading to a class of 1,722,255 particles after initial 2D and 3D classifications. A representative micrograph and top 2D classes are shown in fig. S5. The 3D nonuniform refinement with C2 symmetry for this initial class generated a reconstruction with a nominal resolution of 3.57 Å, based on the Fourier shell correlation (FSC) cutoff at 0.143 between the two half maps (*39*). However, the effective resolution was lower based on visual inspection of the cryo-EM map. The particles were imported to RELION (*40*) for further 3D classification.

The further classification generated a 3D class with a much smaller number of particles (74,320) with a much improved cryo-EM map. The particles were imported back to cryoSPARC for nonuniform refinement, resulting in the final reconstruction of 3.45-Å resolution (3DFSC of 3.47 Å) (fig. S6A). Local resolution variation was estimated in cryoSPARC (fig. S6B). The final map was of excellent quality consistent with the resolution (fig. S6C).

Model building and refinement

The structures of CypA [Protein Data Bank (PDB) 3K0N] and EloB/C (extracted from PDB 3DCG) were docked into the cryo-EM map using Chimera (*41*). The structure of MVV Vif was manually built on the basis of the secondary structure prediction. The complex model was further adjusted in COOT (*42*) with intervening cycles of real-space refinement in PHENIX (*43*) with secondary structure restraints (*44*). The final model with good geometry and fit to the map (fig. S6C, right) was validated using the comprehensive cryo-EM validation tool implemented in PHENIX (Table 1) (*43*). All structural figures were generated using PyMol (*45*) and ChimeraX (*46*).

Supplementary Materials

This PDF file includes:

Figs. S1 to S6
References

View/request a protocol for this paper from *Bio-protocol*.

REFERENCES AND NOTES

1. R. J. Gifford, Viral evolution in deep time: Lentiviruses and mammals. *Trends Genet.* **28**, 89–100 (2012).
2. Y. Luo, E. Y. Jacobs, T. M. Greco, K. D. Mohammed, T. Tong, S. Keegan, J. M. Binley, I. M. Cristea, D. Fenyo, M. P. Rout, B. T. Chait, M. A. Muesing, HIV-host interactome revealed directly from infected cells. *Nat. Microbiol.* **1**, 16068 (2016).
3. R. S. Harris, B. D. Anderson, Evolutionary paradigms from ancient and ongoing conflicts between the lentiviral Vif protein and mammalian APOBEC3 enzymes. *PLOS Pathog.* **12**, e1005958 (2016).
4. X. Yu, Y. Yu, B. Liu, K. Luo, W. Kong, P. Mao, X. F. Yu, Induction of APOBEC3G ubiquitination and degradation by an HIV-1 Vif-Cul5-SCF complex. *Science* **302**, 1056–1060 (2003).
5. S. G. Conticello, R. S. Harris, M. S. Neuberger, The Vif protein of HIV triggers degradation of the human antiretroviral DNA deaminase APOBEC3G. *Curr. Biol.* **13**, 2009–2013 (2003).
6. A. M. Sheehy, N. C. Gaddis, M. H. Malim, The antiretroviral enzyme APOBEC3G is degraded by the proteasome in response to HIV-1 Vif. *Nat. Med.* **9**, 1404–1407 (2003).
7. M. Barry, K. Fruh, Viral modulators of cullin RING ubiquitin ligases: Culling the host defense. *Sci. STKE* **2006**, pe21 (2006).
8. J. S. Albin, R. S. Harris, Interactions of host APOBEC3 restriction factors with HIV-1 in vivo: Implications for therapeutics. *Expert Rev. Mol. Med.* **12**, e4 (2010).
9. R. S. LaRue, S. R. Jonsson, K. A. Silverstein, M. Lajoie, D. Bertrand, N. El-Mabrouk, I. Hotzel, V. Andresdottir, T. P. Smith, R. S. Harris, The artiodactyl APOBEC3 innate immune repertoire shows evidence for a multi-functional domain organization that existed in the ancestor of placental mammals. *BMC Mol. Biol.* **9**, 104 (2008).
10. Y. Nakano, H. Aso, A. Soper, E. Yamada, M. Moriwaki, G. Juarez-Fernandez, Y. Koyanagi, K. Sato, A conflict of interest: The evolutionary arms race between mammalian APOBEC3 and lentiviral Vif. *Retrovirology* **14**, 31 (2017).
11. S. R. Jónsson, V. Andrésdóttir, Host restriction of lentiviruses and viral countermeasures: APOBEC3 and Vif. *Viruses* **5**, 1934–1947 (2013).
12. R. S. Larue, J. Lengyel, S. R. Jonsson, V. Andresdottir, R. S. Harris, Lentiviral Vif degrades the APOBEC3Z3/APOBEC3H protein of its mammalian host and is capable of cross-species activity. *J. Virol.* **84**, 8193–8201 (2010).
13. J. Zhang, J. Wu, W. Wang, H. Wu, B. Yu, J. Wang, M. Lv, X. Wang, H. Zhang, W. Kong, X. Yu, Role of cullin-elonginB-elonginC E3 complex in bovine immunodeficiency virus and maedi-visna virus Vif-mediated degradation of host A3Z2-Z3 proteins. *Retrovirology* **11**, 77 (2014).
14. Z. Xiao, E. Ehrlich, Y. Yu, K. Luo, T. Wang, C. Tian, X. F. Yu, Assembly of HIV-1 Vif-Cul5 E3 ubiquitin ligase through a novel zinc-binding domain-stabilized hydrophobic interface in Vif. *Virology* **349**, 290–299 (2006).
15. A. Mehle, E. R. Thomas, K. S. Rajendran, D. Gabuzda, A zinc-binding region in Vif binds Cul5 and determines cullin selection. *J. Biol. Chem.* **281**, 17259–17265 (2006).
16. Y. Yu, Z. Xiao, E. S. Ehrlich, X. Yu, X. F. Yu, Selective assembly of HIV-1 Vif-Cul5-ElonginB-ElonginC E3 ubiquitin ligase complex through a novel SOCS box and upstream cysteines. *Genes Dev.* **18**, 2867–2872 (2004).
17. Z. Zhao, Z. Li, C. Huan, H. Wang, X. Su, W. Zhang, CAEV Vif hijacks ElonginB/C, CYPA and Cullin5 to assemble the E3 ubiquitin ligase complex stepwise to degrade oaA3Z2-Z3. *Front. Microbiol.* **10**, 565 (2019).
18. I. Taniuchi, M. Osato, T. Egawa, M. J. Sunshine, S. C. Bae, T. Komori, Y. Ito, D. R. Littman, Differential requirements for Runx proteins in CD4 repression and epigenetic silencing during T lymphocyte development. *Cell* **111**, 621–633 (2002).
19. J. R. Kane, D. J. Stanley, J. F. Hultquist, J. R. Johnson, N. Mietrach, J. M. Binning, S. R. Jonsson, S. Barelier, B. W. Newton, T. L. Johnson, K. E. Franks-Skiba, M. Li, W. L. Brown, H. I. Gunnarsson, A. Adalbjornsdottir, J. S. Fraser, R. S. Harris, V. Andresdottir, J. D. Gross, N. J. Krogan, Lineage-specific viral hijacking of non-canonical E3 ubiquitin ligase cofactors in the evolution of Vif anti-APOBEC3 activity. *Cell Rep.* **11**, 1236–1250 (2015).
20. R. Yoshikawa, T. Izumi, Y. Nakano, E. Yamada, M. Moriwaki, N. Misawa, F. Ren, T. Kobayashi, Y. Koyanagi, K. Sato, Small ruminant lentiviral Vif proteins commonly utilize cyclophilin A, an evolutionarily and structurally conserved protein, to degrade ovine and caprine APOBEC3 proteins. *Microbiol. Immunol.* **60**, 427–436 (2016).
21. S. F. Gothel, M. A. Marahiel, Peptidyl-prolyl cis-trans isomerases, a superfamily of ubiquitous folding catalysts. *Cell. Mol. Life Sci.* **55**, 423–436 (1999).
22. K. Watashi, K. Shimotohno, Cyclophilin and viruses: Cyclophilin as a cofactor for viral infection and possible anti-viral target. *Drug Target Insights* **2**, 9–18 (2007).
23. T. R. Gamble, F. F. Vajdos, S. Yoo, D. K. Worthylake, M. Houseweart, W. I. Sundquist, C. P. Hill, Crystal structure of human cyclophilin A bound to the amino-terminal domain of HIV-1 capsid. *Cell* **87**, 1285–1294 (1996).
24. M. Lammers, H. Neumann, J. W. Chin, L. C. James, Acetylation regulates cyclophilin A catalysis, immunosuppression and HIV isomerization. *Nat. Chem. Biol.* **6**, 331–337 (2010).
25. Y. Guo, L. Dong, X. Qiu, Y. Wang, B. Zhang, H. Liu, Y. Yu, Y. Zang, M. Yang, Z. Huang, Structural basis for hijacking CBF-β and CUL5 E3 ligase complex by HIV-1 Vif. *Nature* **505**, 229–233 (2014).
26. J. M. Binning, N. M. Chesarino, M. Emerman, J. D. Gross, Structural basis for a species-specific determinant of an SIV Vif protein toward hominid APOBEC3G antagonism. *Cell Host Microbe* **26**, 739–747.e4 (2019).
27. K. M. Knecht, Y. Hu, D. Rubene, M. Cook, S. J. Ziegler, S. R. Jonsson, Y. Xiong, Maedi-visna virus Vif protein uses motifs distinct from HIV-1 Vif to bind zinc and the cofactor required for A3 degradation. *J. Biol. Chem.* **296**, 100045 (2021).
28. K. Luo, Z. Xiao, E. Ehrlich, Y. Yu, B. Liu, S. Zheng, X. F. Yu, Primate lentiviral virion infectivity factors are substrate receptors that assemble with cullin 5-E3 ligase through a HCCH motif to suppress APOBEC3G. *Proc. Natl. Acad. Sci. U.S.A.* **102**, 11444–11449 (2005).
29. I. Paul, J. Cui, E. L. Maynard, Zinc binding to the HCCH motif of HIV-1 virion infectivity factor induces a conformational change that mediates protein-protein interactions. *Proc. Natl. Acad. Sci. U.S.A.* **103**, 18475–18480 (2006).
30. Y. Hu, K. M. Knecht, Q. Shen, Y. Xiong, Multifaceted HIV-1 Vif interactions with human E3 ubiquitin ligase and APOBEC3s. *FEBS J.* **288**, 3407–3417 (2021).
31. S. R. Franzdottir, K. Olafsdottir, S. R. Jonsson, H. Strobel, O. S. Andresson, V. Andresdottir, Two mutations in the vif gene of maedi-visna virus have different phenotypes, indicating more than one function of Vif. *Virology* **488**, 37–42 (2016).
32. J. Luban, K. L. Bossolt, E. K. Franke, G. V. Kalpana, S. P. Goff, Human immunodeficiency virus type 1 Gag protein binds to cyclophilins A and B. *Cell* **73**, 1067–1078 (1993).
33. T. Hatziioannou, D. Perez-Caballero, S. Cowan, P. D. Bieniasz, Cyclophilin interactions with incoming human immunodeficiency virus type 1 capsids with opposing effects on infectivity in human cells. *J. Virol.* **79**, 176–183 (2005).
34. C. Liu, J. R. Perilla, J. Ning, M. Lu, G. Hou, R. Ramalho, B. A. Himes, G. Zhao, G. J. Bedwell, I. J. Byeon, J. Ahn, A. M. Gronenborn, P. E. Prevelige, I. Rousso, C. Aiken, T. Polenova, K. Schulten, P. Zhang, Cyclophilin A stabilizes the HIV-1 capsid through a novel non-canonical binding site. *Nat. Commun.* **7**, 10714 (2016).
35. D. A. Bosco, E. Z. Eisenmesser, S. Pochapsky, W. I. Sundquist, D. Kern, Catalysis of cis/trans isomerization in native HIV-1 capsid by human cyclophilin A. *Proc. Natl. Acad. Sci. U.S.A.* **99**, 5247–5252 (2002).
36. D. M. Duda, L. A. Borg, D. C. Scott, H. W. Hunt, M. Hammel, B. A. Schulman, Structural insights into NEDD8 activation of cullin-RING ligases: Conformational control of conjugation. *Cell* **134**, 995–1006 (2008).

37. D. N. Mastronarde, Automated electron microscope tomography using robust prediction of specimen movements. *J. Struct. Biol.* **152**, 36–51 (2005).
38. A. Punjani, J. L. Rubinstein, D. J. Fleet, M. A. Brubaker, cryoSPARC: Algorithms for rapid unsupervised cryo-EM structure determination. *Nat. Methods* **14**, 290–296 (2017).
39. S. H. Scheres, S. Chen, Prevention of overfitting in cryo-EM structure determination. *Nat. Methods* **9**, 853–854 (2012).
40. S. H. Scheres, RELION: Implementation of a Bayesian approach to cryo-EM structure determination. *J. Struct. Biol.* **180**, 519–530 (2012).
41. E. F. Pettersen, T. D. Goddard, C. C. Huang, G. S. Couch, D. M. Greenblatt, E. C. Meng, T. E. Ferrin, UCSF Chimera—A visualization system for exploratory research and analysis. *J. Comput. Chem.* **25**, 1605–1612 (2004).
42. P. Emsley, B. Lohkamp, W. G. Scott, K. Cowtan, Features and development of Coot. *Acta Crystallogr. D Biol. Crystallogr.* **66**, 486–501 (2010).
43. P. V. Afonine, B. P. Klaholz, N. W. Moriarty, B. K. Poon, O. V. Sobolev, T. C. Terwilliger, P. D. Adams, A. Urzhumtsev, New tools for the analysis and validation of cryo-EM maps and atomic models. *Acta Crystallogr. D Struct. Biol.* **74**, 814–840 (2018).
44. P. D. Adams, P. V. Afonine, G. Bunkoczi, V. B. Chen, I. W. Davis, N. Echols, J. J. Headd, L. W. Hung, G. J. Kapral, R. W. Grosse-Kunstleve, A. J. McCoy, N. W. Moriarty, R. Oeffner, R. J. Read, D. C. Richardson, J. S. Richardson, T. C. Terwilliger, P. H. Zwart, PHENIX: A comprehensive Python-based system for macromolecular structure solution. *Acta Crystallogr. D Biol. Crystallogr.* **66**, 213–221 (2010).
45. W. DeLano, The PyMOL Molecular Graphics System (DeLano Scientific, 2002).
46. E. F. Pettersen, T. D. Goddard, C. C. Huang, E. C. Meng, G. S. Couch, T. I. Croll, J. H. Morris, T. E. Ferrin, UCSF ChimeraX: Structure visualization for researchers, educators, and developers. *Protein Sci.* **30**, 70–82 (2021).
47. M. Nakashima, S. Tsuzuki, H. Awazu, A. Hamano, A. Okada, H. Ode, M. Maejima, A. Hachiya, Y. Yokomaku, N. Watanabe, H. Akari, Y. Iwatani, Mapping region of human restriction factor APOBEC3H critical for interaction with HIV-1 Vif. *J. Mol. Biol.* **429**, 1262–1276 (2017).
48. M. Ooms, M. Letko, V. Simon, The structural interface between HIV-1 Vif and human APOBEC3H. *J. Virol.* **91**, e02289-16 (2017).
49. A. Zhen, T. Wang, K. Zhao, Y. Xiong, X. F. Yu, A single amino acid difference in human APOBEC3H variants determines HIV-1 Vif sensitivity. *J. Virol.* **84**, 1902–1911 (2010).

Acknowledgments: We thank S. Wu and J. Lin at Yale cryo-EM facilities and G. Hu and L. Wang for assistance in cryo-EM related work. We thank C. Aiken, A. N. Engelman, and all Xiong laboratory members for discussions. **Funding:** This work was supported by National Institutes of Health grant 5R37AI116313 (Y.X.) and University of Iceland Research Fund (S.R.J.). **Author contributions:** Conceptualization: Y.X. and Y.H. Experimental design: Y.X. and Y.H. Biophysical and biochemical experiments: Y.H., K.M.K., and F.A. Virological experiments: R.B.G. Data analysis: Y.H., Y.X., S.R.J., and R.B.G. Supervision: Y.X. Writing—original draft: Y.H., Y.X., S.R.J., and R.B.G. Writing—review and editing: Y.H. and Y.X. **Competing interests:** The authors declare that they have no competing interests. **Data and materials availability:** The model of the MVV VCBC complex has been deposited in the wwPDB with accession code PDB 7UPN. The cryo-EM maps of the MVV VCBC complex have been deposited in EMDB with accession code EMD-26673. All data needed to evaluate the conclusions in the paper are present in the paper and/or the Supplementary Materials.

Submitted 6 June 2022
Accepted 9 December 2022
Published 13 January 2023
10.1126/sciadv.add3422